Fermi National Accelerator Laboratory

FERMILAB-FN-620

Chromaticity Compensation—Booster Sextupoles

S.A. Bogacz, K.Y. Ng and J.F. Ostiguy

Fermi National Accelerator Laboratory
P.O. Box 500, Batavia, Illinois 60510

May 1994

Operated by Universities Research Association Inc. under Contract No. DE-AC02-76CHO3000 with the United States Department of Energy

Disclaimer

CHROMATICITY COMPENSATION – BOOSTER SEXTUPOLES

S.A. Bogacz, K-Y. Ng and J-F. Ostiguy

Accelerator Physics Department,
Fermi National Accelerator Laboratory*
P.O. Box 500, Batavia, IL 60510

April 1994

The current Booster lattice is studied in the context of full chromaticity compensation in the presence of the sextupole fields generated by the combined function magnets. The sextupole excitation at various energies, found from chromaticity measurements and Booster lattice analysis, was compared with magnetostatic multipole calculations. Both results agree very well and they are consistent with the original design specifications. Two families of correcting sextupole magnets are employed to compensate the sextupole excitations and to adjust the chromaticity (in both planes) to a desired value, which is set by head-tail stability consideration. A brief discussion of the Booster's head-tail instability is carried out via the Sacherer-Vlasov formalism. Analysis of the required correcting sextupole strengths is carried out along the momentum ramp with the measured sextupole excitations of the combined function magnets. The results of our calculation give quantitative insight into the requisite performance of the sextupole magnets. It calls for much stronger sextupole strengths – at the level which can no longer be supported by the present correcting sextupole magnet design. Quantitative assessment of the effect of the stronger compensating sextupoles on the dynamic aperture was carried out in terms of the distortion functions. The requisite sextupole configuration does not significantly enhance the third order resonance stop-band – the dynamic aperture remains at acceptable level.

*Operated by the Universities Research Association, Inc., under a contract with the U.S. Department of Energy

INTRODUCTION – BOOSTER LATTICE

Before we proceed with the chromaticity compensation analysis a brief overview of the current Booster lattice and its basic features is in order. The Booster lattice is made up of 24 identical FDOODFO cells. As illustrated in Figure 1, the cell configuration: horizontally focusing magnet – short drift space – horizontally focusing magnet – horizontally defocusing magnet – long drift space – horizontally defocusing magnet, provides room for the RF cavities within the standard cells. Since the lattice half-cell is not symmetric, the beam size is different in each magnet and, consequently, the focusing strengths of F and D combined function magnets are different. The magnets are assembled in 48 modules (two modules per cell). Apart from the F and D magnets, each module consists of a choke, a capacitor bank, an ion pump, a set of correction magnets and a beam position monitor. Two trim correction magnet packages are placed in each period. Each package contains a horizontal dipole, a vertical dipole, a quadrupole and a skew quadrupole. There are also two families of correcting sextupoles, but they are not considered a part of the correction packages. All Booster corrections elements are air core magnets.

The nominal betatron frequencies in the horizontal and vertical planes are $\nu_h = 6.7$ and $\nu_v = 6.8$, respectively. Therefore, there are no second or third order structure resonances adjacent to the working diamond. The lattice tunes are set by the quadrupole strengths of the combined function magnets (focusing and defocusing). The corresponding quadrupole strengths are given by $k_1 = 2.20\ m^{-1}$ and $-2.77\ m^{-1}$. As was mentioned the Booster lattice includes two families of correcting sextupole magnets (horizontal and vertical) placed at locations, where the corresponding beta functions (horizontal and vertical) reach maximum values. One can see from Figure 2 that the horizontal sextupoles are placed in the short straight section of every other cell, while the vertical correcting sextupoles are placed in groups of three in the long straight sections of three equally spaced cells (cell 2, cell 10 and cell 18).

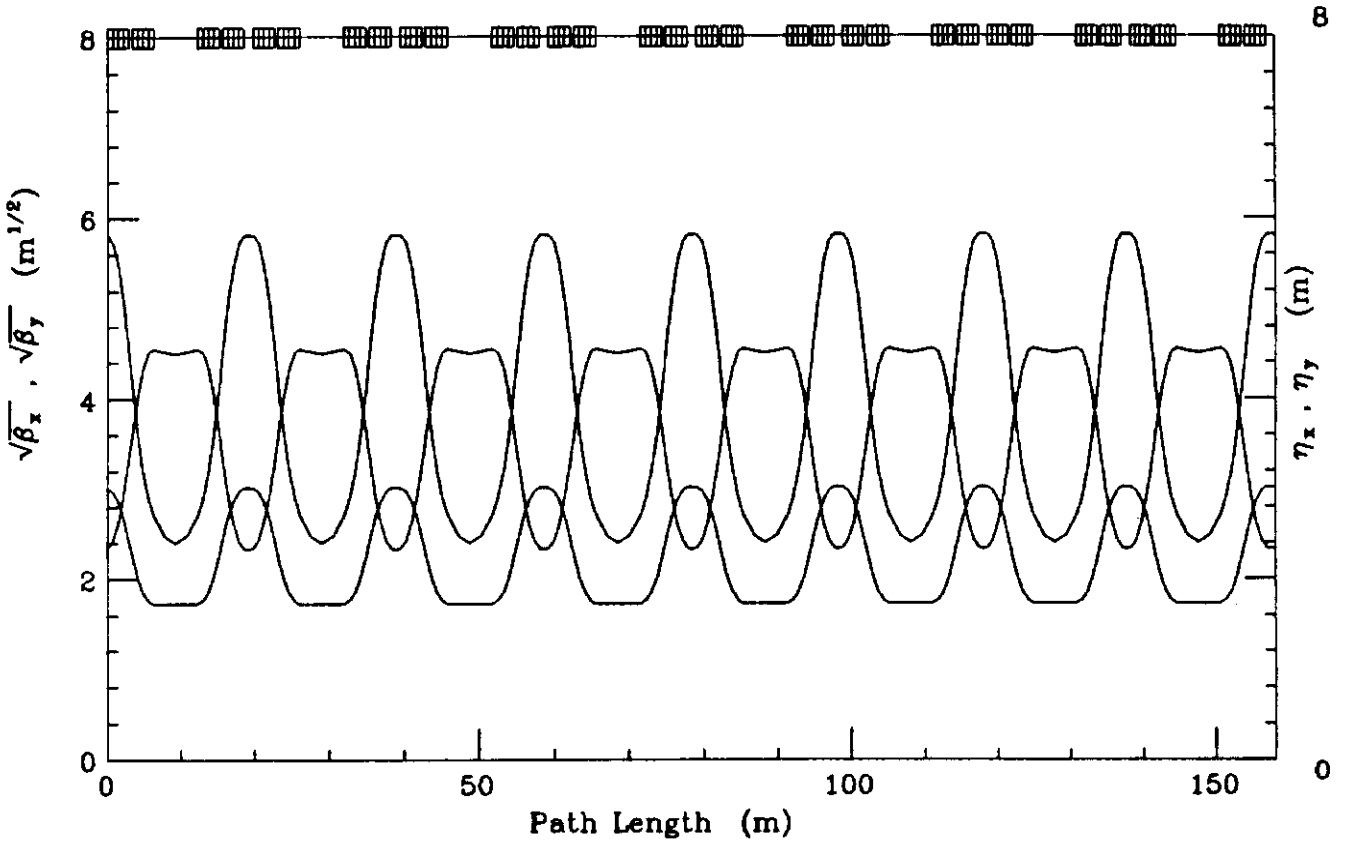
8
6
4
2
0
0
50
100
150
Path Length (m)
$\sqrt{\beta_x}$, $\sqrt{\beta_y}$ (m$^{1/2}$)
η_x , η_y (m)

Figure 1

BOOSTER SEXTUPOLE LAYOUT

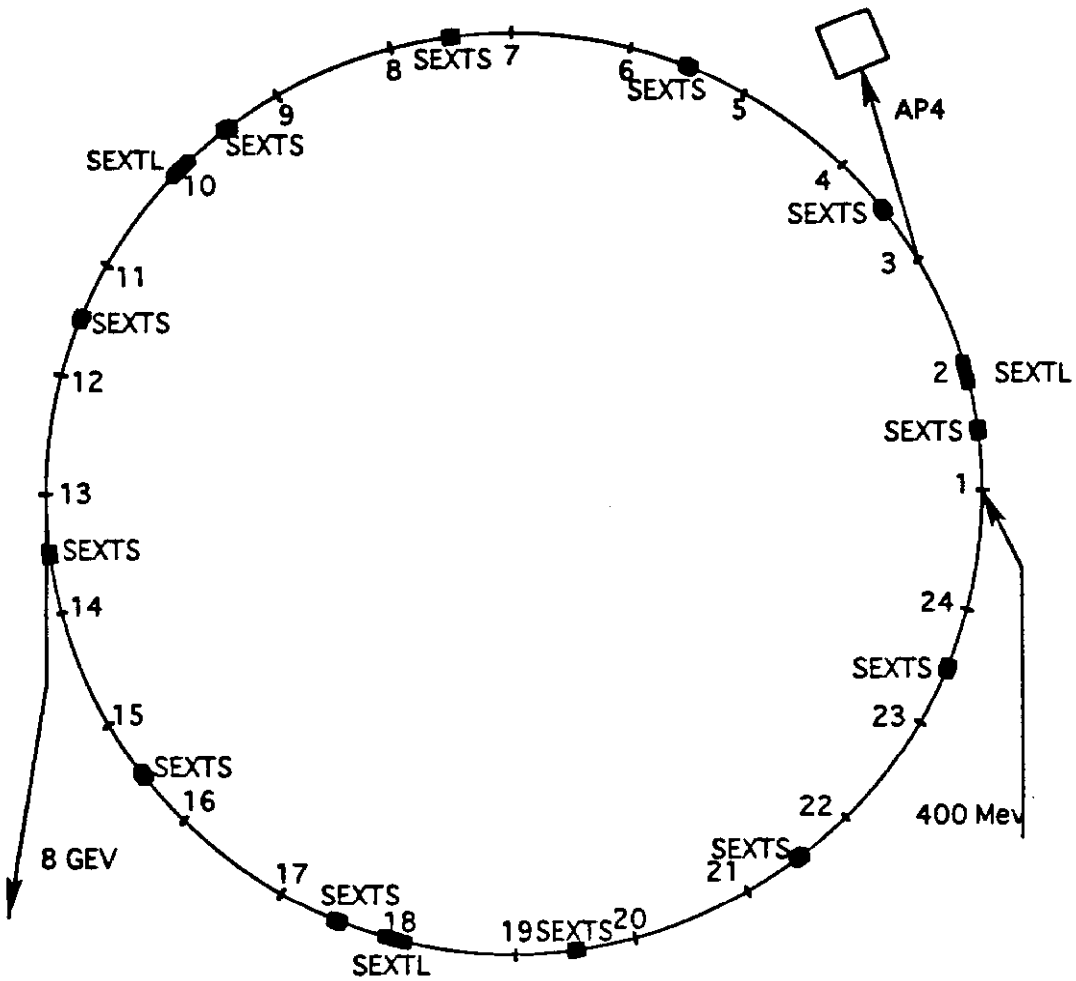

Figure 2

As we will show in this study, more sextupole field is needed to compensate the net chromaticity to the desired level set by head-tail instability present in the Booster. This calls for either stronger sextupole magnets, or for larger number of correcting sextupoles (enhanced lattice). Both options are explored here. Possible performance improvement of the present air core sextupole magnet (enhanced sextupole strength) can be achieved by surrounding a sextupole magnet with an iron shell (to decrease the reluctance of the exterior magnetic path). The maximum enhancement level is estimated using magnetostatic calculation assuming an infinitely thick shell. The second option – putting additional sextupole correctors at various new locations, which have recently opened was also examined. Both options of stronger sextupole compensation were studied from the point of their impact on the dynamic aperture. No significant second order distortions effects were found, which supports our claim that one can safely add more sextupole field.

BOOSTER CHROMATICITY - LINEAR MODEL

The integrated sextupole strength, g, (or S), of an individual sextupole magnet of length L, in Tesla/m (or in geometric units of m^{-2}) is introduced as follows

$$\Delta x' = -\left(\frac{1}{B_o\rho} \int_0^L \frac{1}{2} B''(l)\, dl \right) x^2 = -\frac{1}{B_o\rho}\, g\, x^2 = -\, S\, x^2 \ , \qquad (1)$$

where x, x' are generic coordinates of a transverse phase-space (horizontal or vertical). Here $B_o\rho$ is the magnetic rigidity and B'' is the second derivative of the vertical magnetic field with respect to x.

Apart from two families of correcting sextupoles, there are also additional sextupole fields contributed by the 96 combined function magnets (F and D). The sextupole contribution from a combined function magnet is due primarily to pole geometry and remanent magnetization. Detailed numerical modeling of the multipole content of the F and D magnet geometries is presented in the next section.

For the purpose of our model, the sextupole content of each F and D magnet can be accounted for in the Booster lattice by inserting identical zero-length sextupoles at five equally spaced locations along each magnet. Significant variation of the horizontal and vertical beta functions along the F or D magnet (see Figure 1) calls for distributed sextupole contribution, rather than a lumped sextupole inserted at the middle of the magnet. A discrete five-point-configuration mocks-up sufficiently well continuous distribution of sextupole effect in a realistic Booster magnet (further increasing of number of discrete points yields no chromaticity change). The integrated strength of the sextupole can be conveniently expressed in terms of the normalized sextupole strength, b_2, as follows

$$S = \theta_{bend}\, b_2 \quad ,$$

where (2)

$$b_2 = \frac{1}{B_0 L} \int_0^L \frac{1}{2} B''(l)\, dl \quad .$$

Here θ_{bend} is the bend angle of the combined function magnet.

The goal of the two families of sextupoles (h and v) is to compensate the natural chromaticity, $\underline{\chi}^o$, in the presence of the F and D magnet sextupole excitations, S_F and S_D, to some desired value, $\underline{\chi}$, (both in the horizontal and vertical planes). The following definition of chromaticity is used

$$\Delta\nu = \chi \frac{\Delta p}{p} \quad , \tag{3}$$

where $\Delta\nu$ is the tune shift corresponding to the relative longitudinal momentum offset $\frac{\Delta p}{p}$.

Assuming that the net chromaticity (in both planes) depends linearly on four independent sextupole sources (S_h, S_v, S_F, S_D) one can quite generally write down chromaticity in terms of eight sensitivity coefficients. Using matrix multiplication this relationship assumes the following compact form

$$\underline{\chi} = \underline{\chi}^o + \mathbf{M} \begin{pmatrix} S_h \\ S_v \end{pmatrix} + \mathbf{D} \begin{pmatrix} S_F \\ S_D \end{pmatrix} \quad . \tag{4}$$

Here, the underlined symbols denote 2-dim column vectors (their components correspond to the horizontal and vertical planes). The bold face characters, **M** and **D**, represent two-by-two matrices – one can easily identify the eight sensitivity coefficients with the elements of the two matrices. One can notice in passing,

that both **M** and **D** depend exclusively on the lattice properties. A generic sensitivity coefficient can be expressed in terms of the Twiss functions according to the following relationship

$$M_{\mu\nu} = \frac{1}{2\pi} \sum_{i(\nu)} \beta^{\mu}_{i} \, D^{\mu}_{i} \ . \tag{5}$$

Here, the summation i(ν) goes over locations of all sextupoles of a given family (ν), where β^{μ}_{i} and D^{μ}_{i} are values of the beta function and dispersion at those locations (μ indicates either horizontal or vertical Twiss functions).

Solving Eq.(3) with respect to the correcting sextupole strengths $\underline{g}$ (in Tesla/m) yields the following formula

$$\underline{g} = (B_o\rho)\, \mathbf{M}^{-1} \left[\underline{\chi} - \underline{\chi}^{o} - \mathbf{D} \begin{pmatrix} S_F \\ S_D \end{pmatrix} \right]. \tag{6}$$

The above expression will be used to analyze the required sextupole strength as a function of changing momentum along the Booster ramp. The sensitivity coefficients for all four families of sextupoles, **M** and **D**, are simulated for the Booster lattice using MAD tracking code[1] (version 8.71). The resulting sensitivity coefficients along with the natural chromaticity, $\underline{\chi}^{o}$, are listed below

$$\mathbf{M} = \begin{pmatrix} 1.94 & 0.15 \\ -0.31 & -0.53 \end{pmatrix} \times 10^2,$$

$$\mathbf{D} = \begin{pmatrix} 6.20 & 1.71 \\ -1.58 & -2.59 \end{pmatrix} \times 10^2, \tag{7}$$

$$\underline{\chi}^{o} = \begin{pmatrix} -8.02 \\ -6.76 \end{pmatrix}.$$

To complete the sextupole strength analysis, outlined by Eq.(6), one has to gain some insight into the sextupole excitations of the combined function magnets (F and D) and their variation with the B-field. This will be discussed in detail in the next section via magnetostatic simulation for both geometries of the F and D magnets.

Another independent way of obtaining information about the sextupole excitation of the combined function magnets comes from the beam measurement. Using available chromaticity measurement[2] with both families of correcting sextupoles (h and v) turned off, one can calculate the sextupole excitations of the F and D magnets at various energies along the ramp. This information could be recovered by solving Eq.(4) with respect to S_F and S_D. The corresponding expression is given below:

$$\begin{pmatrix} S_F \\ S_D \end{pmatrix} = \mathbf{D}^{-1} \left[\underline{\chi} - \underline{\chi}^{o} - \frac{1}{B_o \rho} \mathbf{M} \underline{g} \right] \tag{8}$$

Since the correcting sextupoles are off, $\underline{g} = 0$, the above equation reduces to

$$\begin{pmatrix} S_F \\ S_D \end{pmatrix} = \mathbf{D}^{-1} \left[\underline{\chi} - \underline{\chi}^{o} \right] \tag{9}$$

The chromaticity measurements at various energies are illustrated in Figure 3 along with the sextupole excitations curves obtained from these measurements via Eq.(9), with the sensitivity matrix **D** obtained numerically via MAD as given by Eq.(7). These results will be compared with a magnetostatic calculation of the effects of pole geometry and remanent magnetization on the sextupole excitations for the F and D combined function magnets.

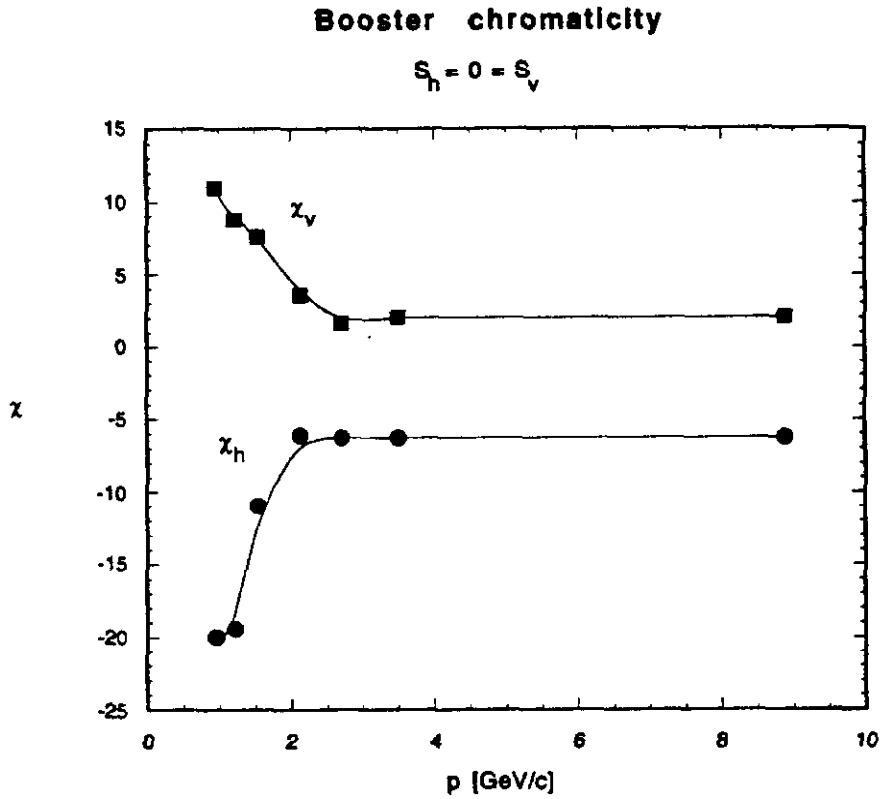
Booster chromaticity
$S_h = 0 = S_v$
χ_v
χ_h
χ
p [GeV/c]

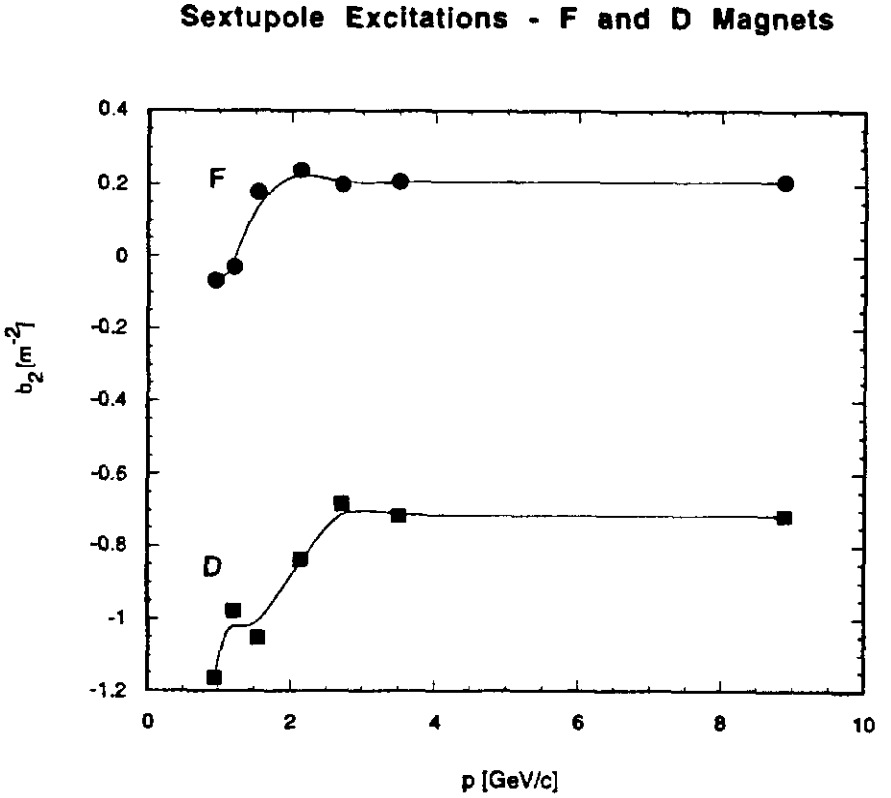
Sextupole Excitations - F and D Magnets
F
D
$b_2 [m^{-2}]$
p [GeV/c]

Figure 3

SEXTUPOLE CONTENT OF THE COMBINED FUNCTION MAGNETS

The bending guide field in the Booster synchrotron is provided by 96 combined function magnets, each approximately 3 m long. The magnetic field varies from approximately 500 Gauss at injection up to 7000 Gauss at extraction. The magnets are powered in a resonant circuit by a 15 Hz sinusoidal waveform resulting in a field of the form

$$B(t) = B_{min} + \frac{1}{2}(B_{max} - B_{min})[1 - \cos(\omega t)] \quad . \tag{10}$$

The Booster D and F magnets cross-sections[3] are shown in Figure 4. It should be noted that these magnets are not mirror images of one another. While the F magnet has a horizontal good field width of 4.3 inch and a vertical aperture of 1.64 inch the corresponding dimensions for the D magnet are 3 inch and 2.25 inch respectively.

One of the technical difficulties in a conventional low energy synchrotron is the field quality degradation at low energy due to remanent fields. For a simple uniform gap configuration, one can easily show, using Ampere's law, that the remanent field is

$$B_r = -\mu_0 H_c \frac{\Lambda}{g} \quad , \tag{11}$$

where g is the pole gap, Λ is the path in iron and H_c is the average coercivity along this path. For a typical magnet, $\frac{\Lambda}{g}$ is of the order of 10 – 20 and $\mu_0 H_c$ is of the order of 1 Gauss. One therefore expects a dipole field of the order of 10 – 20 Gauss. For the Booster magnets, this might represent 1 – 5% of the bending field at injection. Aside from the obvious effect on the dipole component of the field, one also expects, because of the finite extent of the pole face, the remanent magnetization to contribute a negative sextupole component to the field.

Booster 'F' Magnet

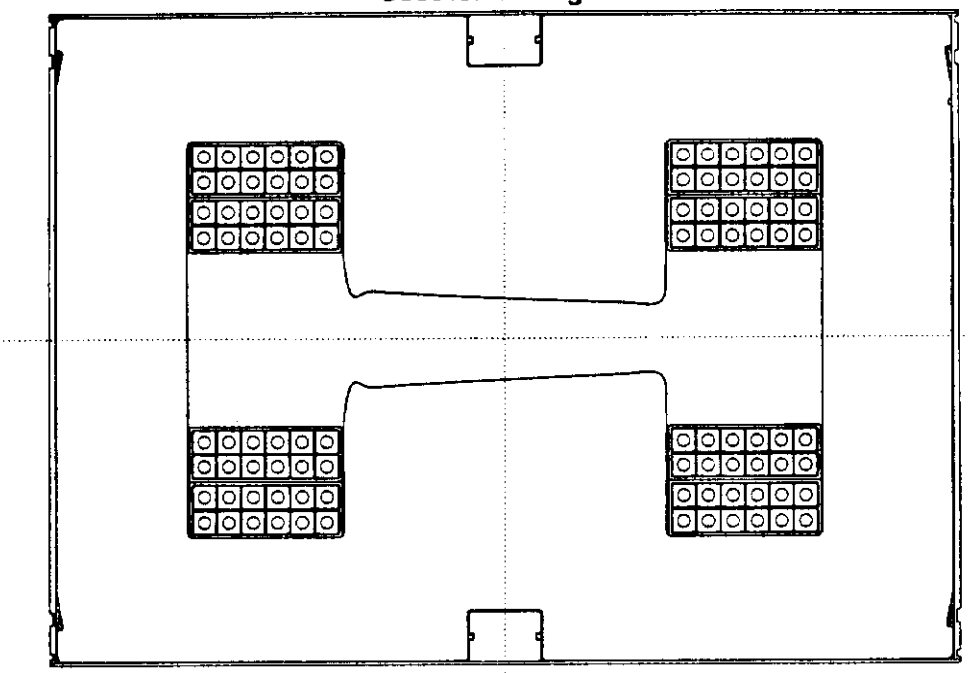

Booster 'D' Magnet

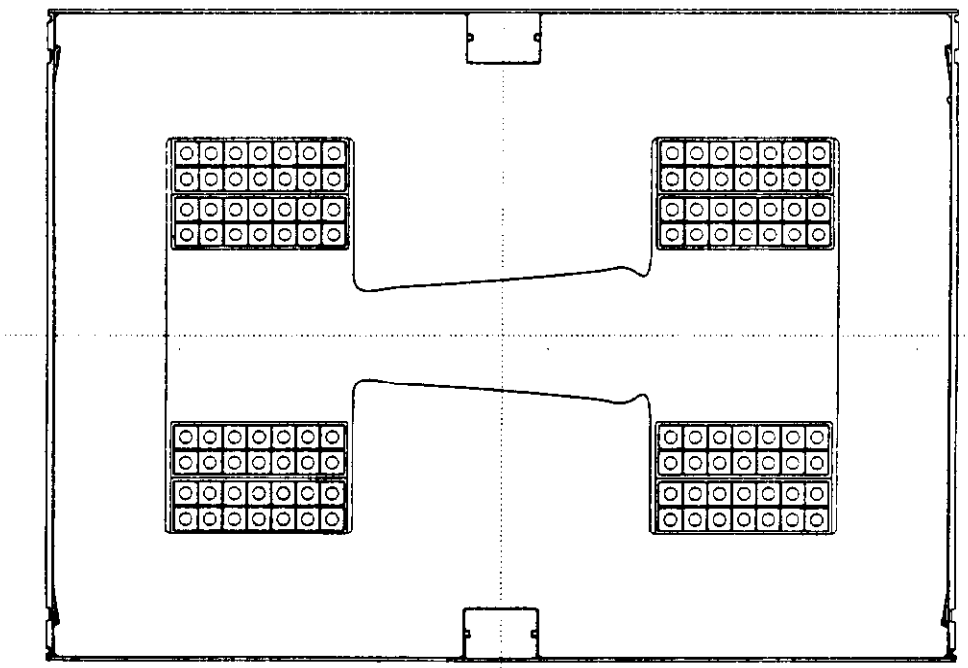

Figure 4

The distinctive characteristic of the remanent magnetization contribution is that it tends to be relatively independent from the excitation. Therefore, when normalized with respect to the main field, the relative contributions from the remanent magnetization to the magnetic field are expected to gradually be reduced to zero as the excitation current is increased from its minimum to its maximum value.

Calculations were performed using a standard finite element code (PE2D). The results are presented in Table 1 and 2. They confirmed the design dipole and focusing strength. Furthermore, higher multipole values (up to the 24-pole) were also calculated for both F and D magnets. In both tables, the multipoles are normalized values at 1 inch. For the D magnet, the calculated dipole field was 6.65239×10^2 Gauss with an excitation of 1518 Ampere-turn and 6.18884×10^3 Gauss for an excitation of 14145 Ampere-turn. For the F magnet, 8.31474×10^2 Gauss for 1384 Ampere-turn and 7.68313×10^3 Gauss for 12900 Ampere-turn. Complete magnetic field profiles for both F and D magnets based on the calculated multipole content are illustrated in Figures 5 and 6.

The Booster magnets are operated well below saturation and not surprisingly, the calculations show that there is no significant dependence of the field harmonics on the excitation current. The magnitudes of the dipole and quadrupole components of the field are in excellent agreement with the design values. The sextupole component (the third row in Tables 1 and 2) can be easily converted into b_2, defined in Eq.(2), simply by dividing them by $2.54^2 \times 10^4$. After conversion, the simulated values of b_2 in $[m^{-2}]$ are given as follows: 2.41×10^{-5}, for the F magnet and -6.24×10^{-5} for the D magnet. As explained before, the sextupole component of the bending magnet magnetic field can be extracted from a beam-based chromaticity measurement (see Figure 3). The beam-based (measured) values of b_2 in $[m^{-2}]$ are listed as: 2.0×10^{-5} for the F magnet and -6.9×10^{-5} for the D magnet. One can see that the calculated sextupole components at 8 GeV are in good agreement with the values inferred from chromaticity measurements.

Booster F magnet multipoles ($\times 10^4$) (normalization radius = 1 inch)		
pole	Injection	Extraction
2	1.00000×10^{4}	1.00000×10^{4}
4	5.62210×10^{2}	5.62409×10^{2}
6	1.42220×10^{0}	1.55437×10^{0}
8	3.38836×10^{-2}	3.47808×10^{-2}
10	6.73212×10^{-1}	6.85997×10^{-1}
12	-4.33973×10^{-1}	-4.36889×10^{-1}
14	-1.08279×10^{0}	-1.11523×10^{0}
16	6.44508×10^{-1}	6.84466×10^{-1}
18	1.17022×10^{0}	1.15652×10^{0}
20	1.92633×10^{-1}	3.86541×10^{-1}
22	-8.00929×10^{-1}	-9.04634×10^{-1}
24	-2.47537×10^{0}	-2.37865×10^{0}

Table 1

Booster D magnet multipoles ($\times 10^4$) (normalization radius = 1 inch)		
pole	Injection	Extraction
2	1.00000×10^{4}	1.00000×10^{4}
4	-7.02859×10^{2}	-7.02743×10^{2}
6	-3.91965×10^{0}	-4.02587×10^{0}
8	-2.98606×10^{-1}	-2.95847×10^{-1}
10	4.49709×10^{-1}	4.37877×10^{-1}
12	2.77620×10^{-1}	2.70908×10^{-1}
14	8.44590×10^{-2}	7.02125×10^{-2}
16	-2.13484×10^{-1}	-2.11247×10^{-1}
18	4.47200×10^{-2}	4.20609×10^{-2}
20	1.93170×10^{-1}	2.02255×10^{-1}
22	-1.16070×10^{-2}	-9.91963×10^{-3}
24	-1.73761×10^{-1}	-1.62111×10^{-1}

Table 2

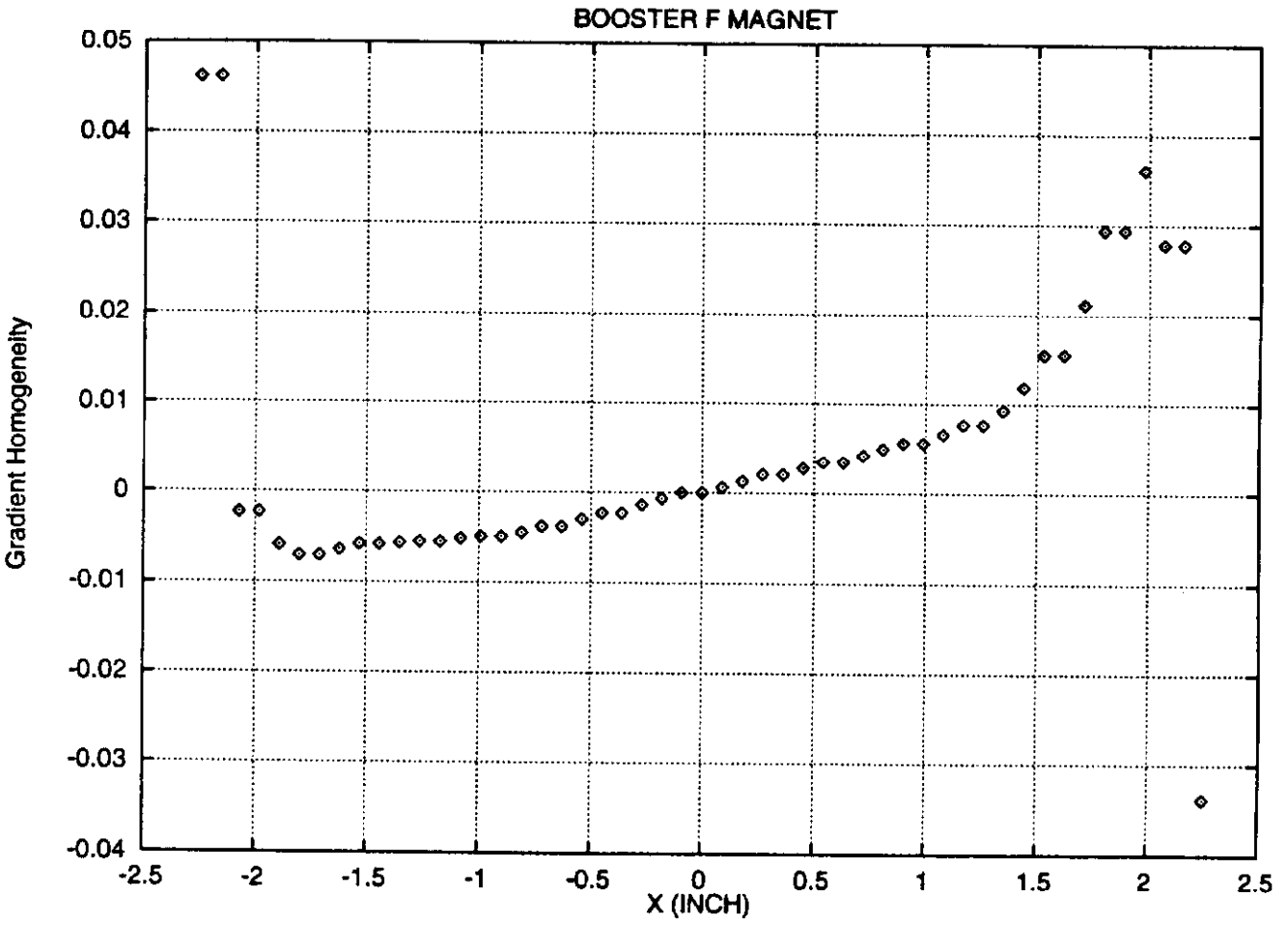
BOOSTER F MAGNET
Gradient Homogeneity
0.05
0.04
0.03
0.02
0.01
0
-0.01
-0.02
-0.03
-0.04
-2.5
-2
-1.5
-1
-0.5
0
0.5
1
1.5
2
2.5
X (INCH)

Figure 5

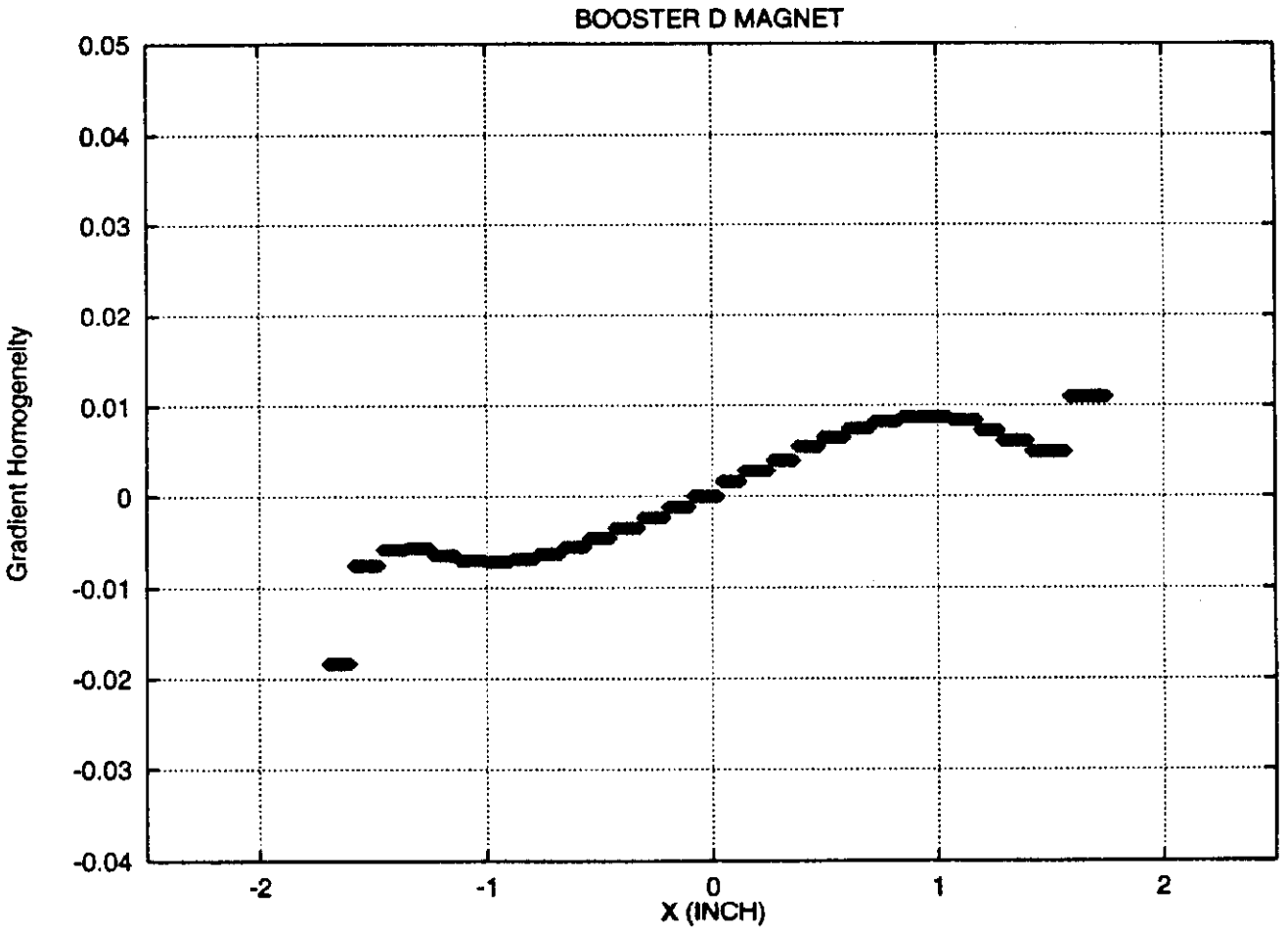
BOOSTER D MAGNET
Gradient Homogenelty
0.05
0.04
0.03
0.02
0.01
0
-0.01
-0.02
-0.03
-0.04
-2
-1
0
1
2
X (INCH)

Figure 6

The small difference in b_2's ($0.4 \times 10^{-5}\ m^{-2}$ for the F magnet and $0.6 \times 10^{-5}\ m^{-2}$ for the D magnet) can be attributed to the fact that the sextupole obtained from beam based measurement includes magnet end contributions, while the magnetostatic calculation is strictly 2-dimensional and it accounts only for the 'body' contribution to the multipoles. At injection energy (200 MeV), the sextupole components for both the D and F magnets are more negative than the magnetostatic prediction.

The difference between the values at injection and extraction is to be interpreted as a measure of the remanent magnetization contribution to the sextupole. These values of remanent sextupole component b_2 in [m^{-2}], inferred from Figure 3, are given as follows: 2.7×10^{-5}, for the F magnet and 4.9×10^{-5} for the D magnet. The information provided by the beam-based measurement is extremely valuable since it is difficult to calculate remanent magnetization effects. The good agreement between the calculated sextupole components and the ones derived from the beam-based chromaticity measurement at 8 GeV makes one relatively confident that the beam-based chromaticity measurements[2] are correct.

POTENTIAL IMPROVEMENTS TO AIR CORE SEXTUPOLES

It has been suggested to increase the strength of the existing air-core chromaticity correction sextupole magnets by introducing an external iron shell. This is illustrated schematically in Figure 7. The field enhancement effect due to an iron shell can be estimated by using the following result: for a filament of current located at (ρ, ϕ) inside a circular hole of radius R carved into a medium of relative permeability μ the complex coefficients $C_n e^{i\alpha_n}$ – the multipole expansion of the field are given below[4]

$$\frac{C_n e^{i\alpha_n}}{R^{n-1}} = -\frac{\mu_0}{2\pi} \int \frac{dI}{\rho^n} \left[1 + \frac{\mu - 1}{\mu + 1} \frac{\rho^{2n}}{R^{2n}}\right] e^{in\phi} . \tag{12}$$

For a pure sextupole current layer of inner radius a and outer radius b, with a uniform current density given by

$$J_3(\rho,\phi) = J_3 \cos 3\phi \tag{13}$$

one can easily carry out the integration in the right hand side of Eq.(12), which reduces to the following simple expression

$$\frac{C_3}{R^2} = -\frac{\mu_0 J_3}{2} \left[\frac{b - a}{ab} + \frac{\mu - 1}{\mu + 1} \frac{b^5 - a^5}{5R^6}\right] . \tag{14}$$

Under ideal conditions, i.e. $\mu = \infty$ (μ is about 100 for iron) and a = b = R, the sextupole field could be doubled. More realistically, let $a \approx b < R$ and $t = b - a << R$. The above expression, Eq.(14), becomes

$$\frac{C_3}{R^2} = -\frac{\mu_0 J_3 t}{2a^2} \left[1 + \frac{\mu - 1}{\mu + 1} \frac{a^6}{R^6}\right] . \tag{15}$$

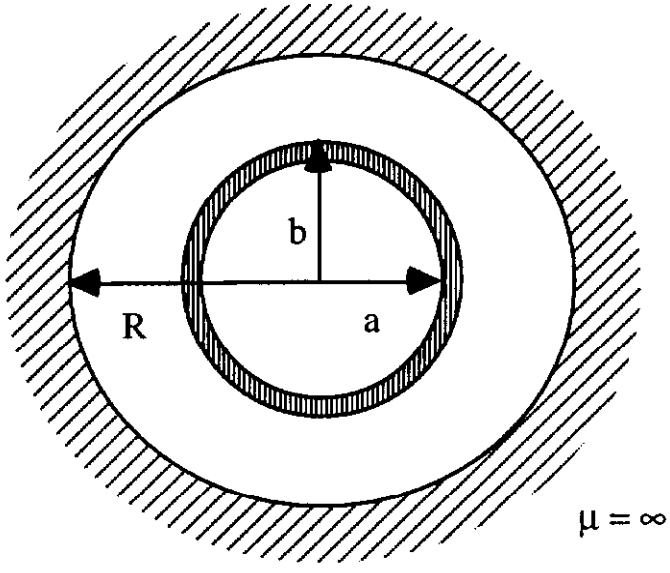

Figure 7

The sextupole field is enhanced roughly by a factor $1 + \left(\frac{a}{R}\right)^6$. It is probably unrealistic to expect an enhancement factor larger than 1.5 in a real device. We note that because the exterior field decays faster as the pole number increases, field enhancement with an iron shell is less effective for a sextupole than for a dipole magnet. One should also consider a new sextupole magnet design – an iron core sextupole – e. g. a similar design to the Main Injector sextupole corrector, with the fast cycling feature taken into account.

HEAD-TAIL INSTABILITY LIMITS

Following Sacherer's argument[5] one can generalize a simple formalism describing a wake field driven coherent betatron motion of a coasting beam to model head-tail instability of the bunched beam. The inverse growth-time of the l-th mode is expressed by the following formula

$$\frac{1}{\tau^l} = -\frac{ce\beta I_o}{4\pi E\nu} \ \mathrm{Re}\ Z^l_{eff} \ , \tag{16}$$

where $E = \gamma m_o c^2$ is the total energy, ν is the betatron tune and β is the average beta function. Here, Z^l_{eff} denotes the effective transverse impedance defined as follows

$$Z^l_{eff} = \frac{2\pi}{l+1} \frac{1}{2\omega_o \hat{\tau}} \sum_{p=-\infty}^{\infty} Z_\perp(\omega_p)\, \rho^l(\omega_p - \omega_\chi) \quad , \tag{17}$$

where $\omega_\chi = \frac{\chi}{\eta}\omega_o$ and $\omega_p = (p+\nu)\omega_o$. Here, $Z_\perp$ denotes the transverse coupling impedance, I_o is the total current of a bunch of length $\hat{\tau}$ (in time units). The following approach assumes 'ad hoc' existence of a given head-tail mode, l, by imposing specific periodic dependence of the betatron motion with respect to the longitudinal position, τ. The beam power spectrum for a given mode is defined as follows

$$\rho^l(\omega) = \frac{h^l(\omega)}{\sum_{p=-\infty}^{\infty} h^l(\omega_p - \omega_\chi)} \ . \tag{18}$$

The explicit form of the power spectrum of a sinusoidal mode, as assumed by Sacherer, is given by the following expression

$$h^{l}(\omega) = \frac{4}{\pi^2}\ (l+1)\ \frac{1 + (-1)^{l} \cos(2\omega\hat{\tau})}{\left[(2\omega\hat{\tau}/\pi)^2 - (l+1)^2\right]^2}\ . \tag{19}$$

As discussed in detail in Ref. 6, in order to obtain a substantial effective impedance for relatively small chromaticities ($\chi \sim 10$) one has to start with the transverse impedance, which significantly overlaps with the beam spectrum (see Eq.(18)–(19)). We tentatively identified kicker magnets as a possible source of offending impedance, which possesses the above feature and therefore will contribute substantially to the effective impedance. There are eight kicker magnets; both injection, extraction and abort kickers located around the ring. The real part of the transverse coupling impedance of a kicker of half-width a, half-height b and length L is given by the following analytic expression[6]

$$\mathrm{Re}\, Z_{\perp}(\omega) = \frac{Z_0 L}{4ab}\ \frac{1}{\omega}\ \left(1 - \cos\frac{\omega L}{c}\right)\ , \tag{20}$$

where for the Booster's kickers the following list of parameters holds:

$$\begin{aligned} Z_0 &= 377\ \text{Ohm} \\ L &= 2\ \text{m} \\ a &= 3.7\ \text{cm} \\ b &= 1.9\ \text{cm}. \end{aligned} \tag{21}$$

The transverse impedance spectrum described by Eq.(20) has a primary maximum centered at frequency $\omega_r = \pi c/L$ followed by a set of secondary maxima. The maximum value and the center frequency of the peak, evaluated according to kicker parameters, Eq.(21), are given by

$$\mathrm{Re}\,(Z_\perp)^{max} = \frac{Z_0 L}{4ab}\,\frac{1}{\omega_r} \approx 2.3 \times 10^{-3}\ \mathrm{Ohm/m}\ ,$$

and

$$\omega_r = \frac{\pi c}{L} \approx 500\ \mathrm{MHz}\ . \tag{22}$$

The inverse growth-time as a function of chromaticity was evaluated for different slow head-tail modes (l = 0, 1, 2, 3) according to Eqs.(16)–(19). They are illustrated in Figure 8. As one can see, the l = 0 mode appears to be unstable above transition for small negative chromaticities and might lead to significant enhancement of coherent betatron motion. The obvious cure to stabilize the dipole mode is to maintain appropriate sign (positive) of the net chromaticity. Otherwise, this potentially offending mode can be effectively suppressed by the active damper system. This efficient cure for the l = 0 mode obviously does not work in case of the higher modes, since its feedback system picks up only the transverse position of a bunch centroid, which remains zero due to the symmetry of the higher modes. Another possible cure especially effective for the $l \geq 1$ modes would involve the Landau damping, e. g. through the octupole-induced betatron tune spread. Increasing betatron amplitude of initially unstable mode causes increase of the tune spread, which will eventually self-stabilize development of this mode. Here we consider the situation without any active damper system present. Figure 8 shows that a net chromaticity of 7 units would keep stable two dominant modes (l = 0, 1). Therefore, presented head-tail stability analysis suggests adjusting the net chromaticity at −7 (+7) units below (above) transition energy. This result will be used as a starting point for the chromaticity compensation analysis, which will be discussed in the next section.

The above analysis may serve as an effective method of getting useful information about the transverse impedance spectrum. If one measured experimentally the growth rate of the dipole mode as a function of chromaticity, presented formalism would give immediately the absolute value of $\mathrm{Re}\,(Z_\perp)^{max}$ and the location of center frequency, ω_r (see Figure 8). Whether the proposed measurement is feasible is left for further discussion.

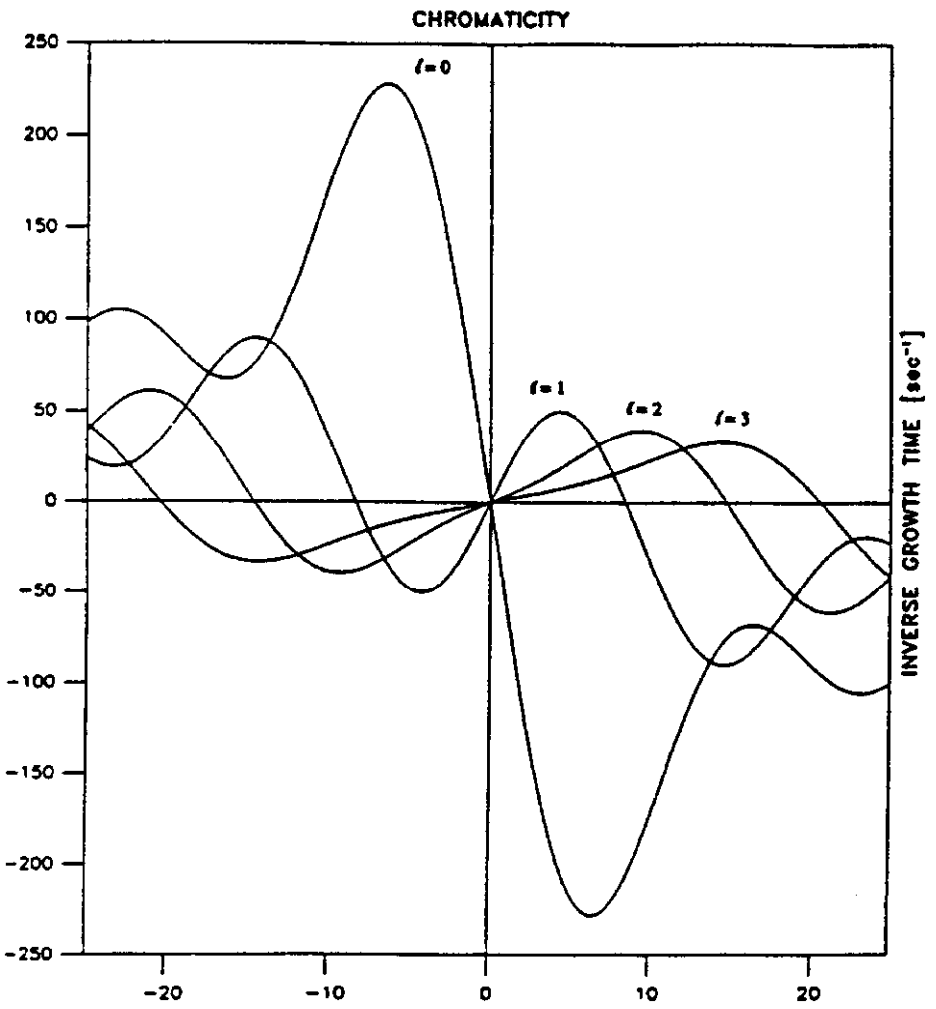

ε = 0.3 eV-sec.

Figure 8

SEXTUPOLE STRENGTH

Now, one can evaluate the correcting sextupole strength, $\underline{g}$, given by Eq.(4), for each value of b_2 taken from Figure 3. This procedure will generate sextupole strength ramps for both families of correcting sextupoles (h and v). Figure 9 summarizes final sextupole requirements for two useful chromaticity compensation scenarios, namely: 1) net chromaticity in both planes flips sign at transition (from −7 chromaticity units before transition to 7 units above transition), 2) zero net chromaticity is maintained throughout the whole ramp. In practice, the chromaticity 'flip' is done over a finite time interval centered around transition. Its duration is governed by the inductance of the sextupole power supplies. One knows from the measurement[3] how the correcting sextupole strengths depend on the electric current. The scaling for the horizontal and vertical correctors are given as follows

$$g_h(I) = 3.6 \times 10^{-3} \times I \quad [\text{Tesla m}^{-1}] \ ,$$

and (23)

$$g_v(I) = 3.1 \times 10^{-2} \times I \quad [\text{Tesla m}^{-1}] \ ,$$

where the current, I, is given in Amperes. Using Eq.(23) one can express content of Figure 9 in terms of current requirements, which is illustrated in Figure 10.

One can see immediately, that with the present values of maximum current supplied to the correcting sextupole magnets (I_{max} = 80 Amperes limited by present power supplies) one could barely compensate chromaticity at the beginning of the ramp. To carry out proposed compensation scheme above transition and eventually throughout the entire ramp one would have to apply sextupole fields at the level much exceeding capability of a present air core sextupole magnet (limited by the maximum current of 280 Amperes), or its upgraded version discussed in one of the previous sections. Without resorting to a new design of the sextupole corrector, which would accommodate requisite level of performance in the present layout of correcting sextupoles, one of the obvious solutions is to put more air core sextupoles at various new

locations. Here, we propose an 'enhanced layout' of correcting sextupoles, which is illustrated in Figure 11. The ideal fully 'enhanced layout' assumes that a horizontal sextupole is placed in every short straight section (in 24 cells), while the vertical correcting sextupoles are placed, as in the present Booster lattice, in groups of three in the long straight sections of three equally spaced cells (cell 2, cell 10 and cell 18), plus a single vertical sextupole placed in every long straight section (in all remaining 21 cells). The above 'enhanced layout' contains total of 24 horizontal sextupoles (present layout – 12) and total of 30 vertical sextupoles (present layout – 9). All horizontal (vertical) correcting sextupoles are placed in equivalent locations (with respect to their sensitivity to chromaticity change) in the lattice – the same values of betas and dispersion functions (see Eq.(5)) in all selected locations. Therefore, the requisite currents illustrated in Figure 10 will scale down according to the above enhancement ratios. The above fully enhanced correcting sextupole layout may have to be compromised due to lack of space in some locations. It was pointed out[7] that every other short straight section is presently occupied by γ_t-jump quadrupoles, which will be needed for transition crossing emittance preservation if coupled-bunch instabilities can be controlled; i.e. transition is not 'jumped' now, because blowing up the longitudinal emittance at transition helps to control the coupled-bunch problem after transition. It may also be difficult to find extra room in the long straight sections containing doublets of r.f. cavities. In a realistic sextupole layout, in odder to achieve the desired net chromaticity compensation, one would have to scale up correcting strengths according to the actual number of correcting sextupoles (in a linear fashion).

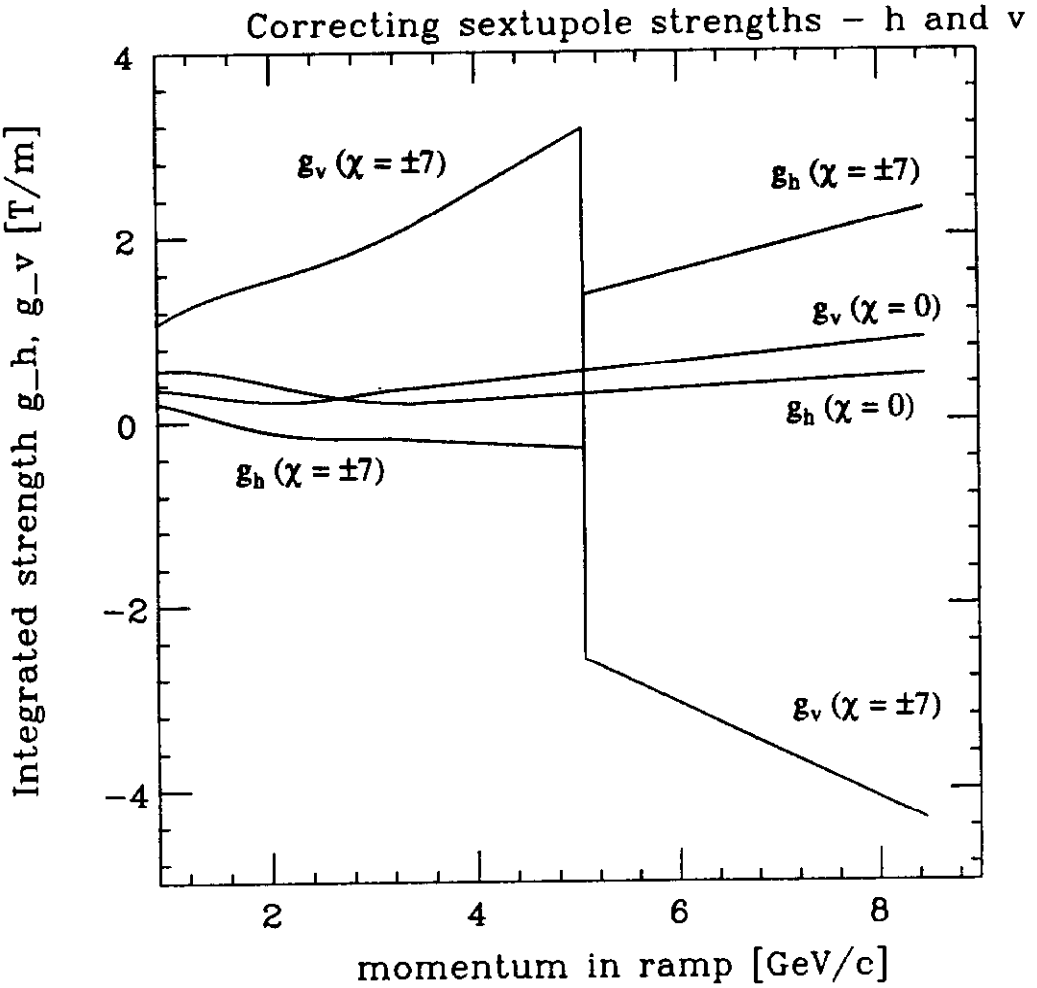
Correcting sextupole strengths – h and v
Integrated strength g_h, g_v [T/m]
momentum in ramp [GeV/c]
g_v ($\chi = \pm 7$)
g_h ($\chi = \pm 7$)
g_v ($\chi = 0$)
g_h ($\chi = 0$)
g_h ($\chi = \pm 7$)
g_v ($\chi = \pm 7$)
4
2
0
−2
−4
2
4
6
8

Figure 9

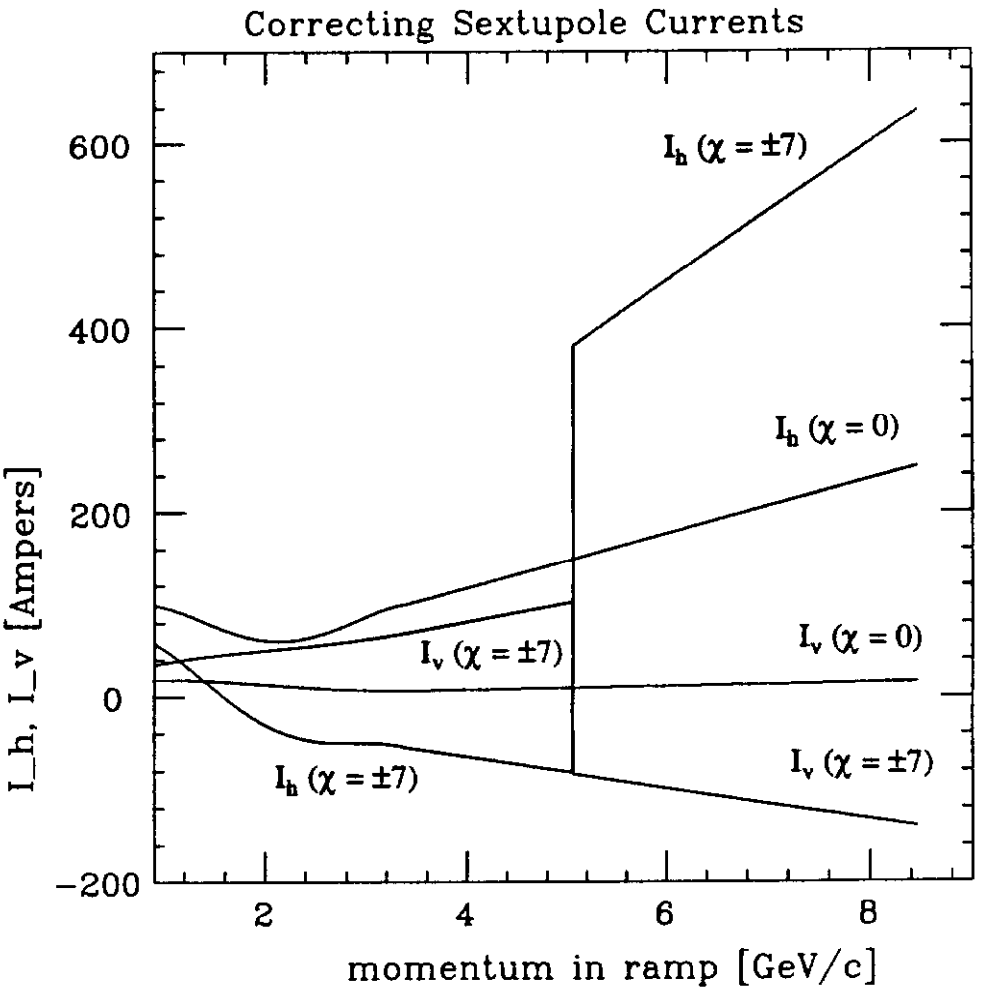
Correcting Sextupole Currents
600
400
200
0
−200
I_h, I_v [Ampers]
2
4
6
8
momentum in ramp [GeV/c]
I_h (χ = ±7)
I_h (χ = 0)
I_v (χ = ±7)
I_v (χ = 0)
I_h (χ = ±7)
I_v (χ = ±7)

Figure 10

BOOSTER SEXTUPOLE LAYOUT

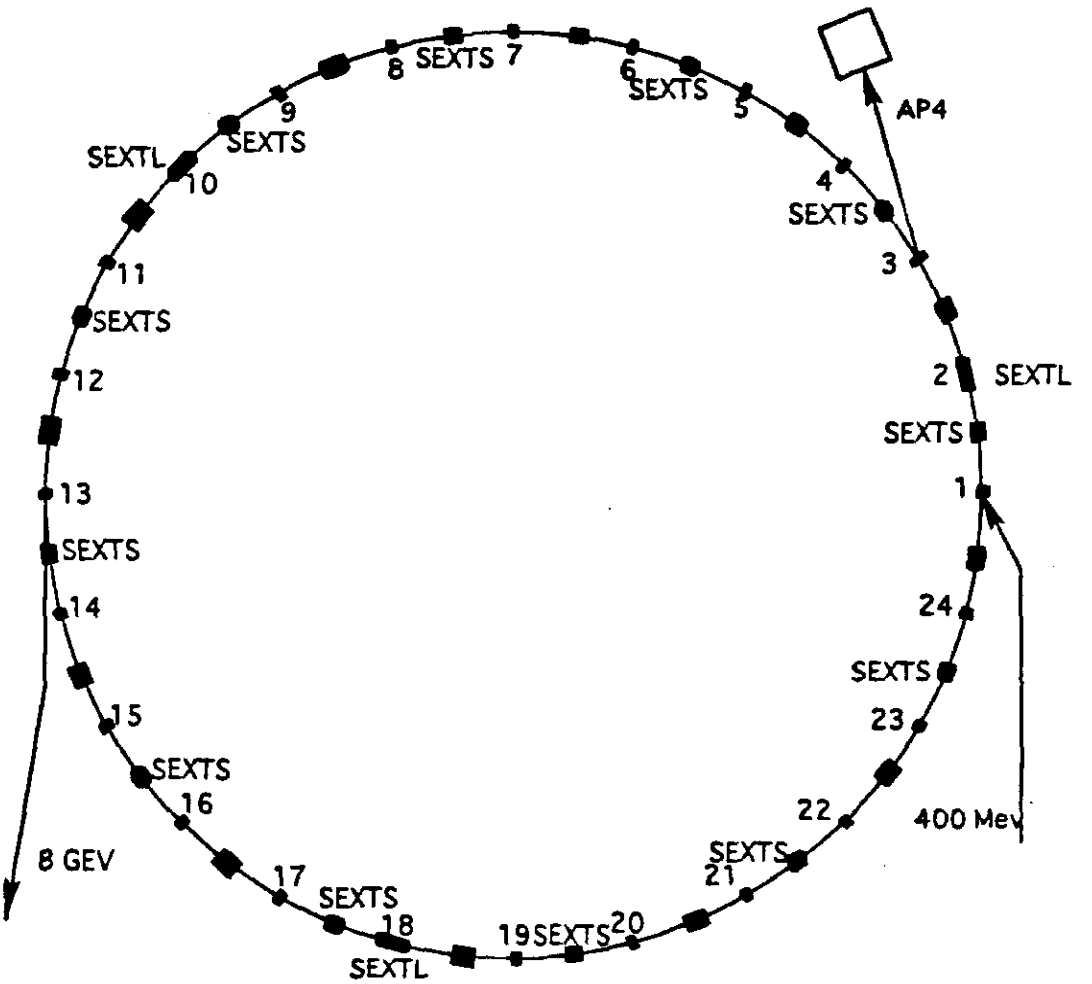

Figure 11

NONLINEARITY CREATED BY SEXTUOPLES – DISTORTION FUNCTIONS ASSESSMENT

The presence of correction sextupoles creates nonlinearity in the Booster lattice. Except near a resonance, this nonlinearity is best described by a set of distortion functions introduced by Collins[8]. They are analogous to the beta functions accounting for presence of quadrupoles. The distortion functions come in five sets (A_1, B_1), (A_3, B_3), $(\bar{A}, \bar{B})$, (A_+, B_+) and (A_-, B_-). The A's are in fact derivatives of the B's. The distortion functions are periodic functions around the ring, they rotate as vectors according to the angles, ϕ_x, $3\phi_x$, ϕ_x, $2\phi_x + \phi_y$, and $2\phi_y - \phi_x$, respectively, where ϕ_x and ϕ_y are the horizontal and vertical Floquet phases. Along a thin sextupole of strength S, defined according to Eq.(1), the B's are continuous, while the first two A's and the last three A's have discontinuities given below[9]

$$\Delta A = \frac{1}{4} \beta_x^{3/2} S , \tag{24}$$

and

$$\Delta \bar{A} = \frac{1}{4} \beta_x^{1/2} \beta_y S , \tag{25}$$

respectively, where β_x and β_y are the beta functions at the sextupole.

The first-order effect of the sextupoles is a change in the transverse beam profile. Locally, at a position along the ring where the beta functions are β_x and β_y, the horizontal and vertical displacements, Δx and Δy, of a particle at the edge of the beam are given by[10]

$$\frac{\Delta x}{\sqrt{\beta_x}} = \frac{\varepsilon_x}{\pi} \left[\left(A_3 \sin 3\varphi_x - B_3 \cos 3\varphi_x \right) - \left(A_1 \sin 3\varphi_x - B_1 \cos 3\varphi_x \right) \right] \tag{26}$$

$$- \frac{\varepsilon_y}{\pi} \left[\left(A_+ \sin\varphi_+ - B_+ \cos\varphi_+ \right) - \left(A_- \sin\varphi_- - B_- \cos\varphi_- \right) \right] ,$$

and

$$\frac{\Delta y}{\sqrt{\beta_y}} = -\ 2\sqrt{\frac{\varepsilon_x}{\pi}}\sqrt{\frac{\varepsilon_y}{\pi}}\left[\left(A_+\sin\varphi_+ - B_+\cos\varphi_+\right) + \left(A_-\sin\varphi_- - B_-\cos\varphi_-\right)\right] \ , \qquad (27)$$

where $\varphi_\pm = 2\varphi_y \pm \varphi_x$ and φ_x, φ_y are the instantaneous horizontal and vertical betatron phases. Assuming a horizontal and vertical normalized emittance of $\varepsilon_x = \varepsilon_y = 10\pi$ mm–mrad, we vary ϕ_x and ϕ_y to find the maximum extra excursion of a beam particle at the edge of the bunch for every point along the the Booster ring. Here we consider the 'enhanced' sextupole layout – 24 horizontal sextupoles at the short straights, 3 vertical sextupoles each at 3 long straights, and one vertical sextupole each at the other 21 long straights. These sextupole strengths are adjusted to produce horizontal and vertical chromaticities of $\chi_x = \chi_y = 7$ near extraction. The result is plotted in Figure 12. We see that the maximum extra excursion is only about 0.6 mm horizontally and 0.4 mm vertically.

The second-order sextupole effect is tune dependent on amplitudes, which can be written in terms of the distortion functions as follows

$$\Delta\nu_x = -\frac{\varepsilon_x}{4\pi^2}\sum_k \left(B_3 s + 3B_1 s\right)_k - \frac{\varepsilon_y}{2\pi^2}\sum_k \left(B_+\bar{s} + B_-\bar{s} - 2B_1\bar{s}\right)_k \ , \qquad (28)$$

and

$$\Delta\nu_y = -\frac{\varepsilon_x}{2\pi^2}\sum_k \left(B_+\bar{s} + B_-\bar{s} - 2B_1\bar{s}\right)_k - \frac{\varepsilon_y}{4\pi^2}\sum_k \left(B_+\bar{s} - B_-\bar{s} + 4\bar{B}\bar{s}\right)_k \ , \qquad (29)$$

where the summations are carried over all sextupoles. With the above described (enhanced) arrangement of sextupoles, we obtain

$$\nu_x = 6.9393 + 39.9\,\frac{\varepsilon_x}{\pi} - 29.1\,\frac{\varepsilon_y}{\pi} \ ,$$

and (30)

$$\nu_y = 6.6653 - 29.1\,\frac{\varepsilon_x}{\pi} - 12.1\,\frac{\varepsilon_y}{\pi} \ ,$$

where ε_x and ε_y, are in units of mm-mrad. With emittances of 10π mm–mrad, the tune spreads due to sextupole nonlinearity are only ~ 0.0001 in the horizontal and ~0.0004 in the vertical directions.

For comparison, the above analysis was carried out for the present configuration of correcting sextupoles – 12 horizontal sextupoles at the short straights and 3 vertical sextupoles each at 3 long straights. Assuming the same net chromaticity compensation at extraction part of the Booster ramp (7 chromaticity units in both planes), which could be achieved with much stronger iron core sextuople magnets, the resulting sextupole tune-shifts are given as follows

$$\Delta\nu_x = 91.1 \frac{\varepsilon_x}{\pi} - 77.82 \frac{\varepsilon_y}{\pi} ,$$

and (31)

$$\Delta\nu_y = -77.82 \frac{\varepsilon_x}{\pi} - 18.75 \frac{\varepsilon_y}{\pi} .$$

With emittances of 10π mm–mrad, the tune spreads due to sextupole nonlinearity are much larger, but still acceptable. Similarly, for this case, we vary φ_x and φ_y to find the maximum extra excursion of a beam particle at the edge of the bunch for every point along the Booster ring. The results, summarized in Figure 13, show larger excursion of particles in a beam as one may expect.

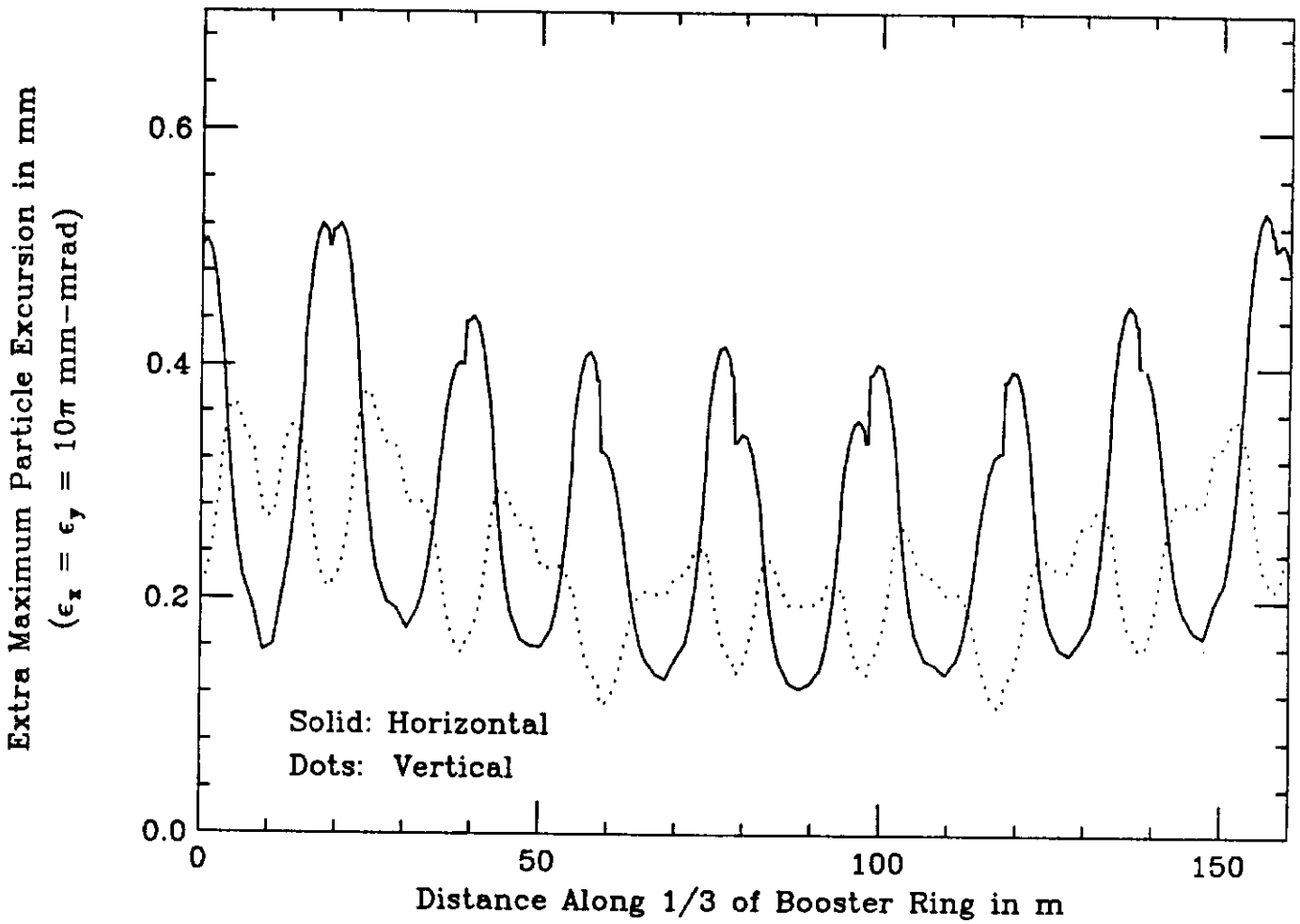
Extra Maximum Particle Excursion in mm
($\epsilon_x = \epsilon_y = 10\pi$ mm-mrad)
0.6
0.4
0.2
0.0
0
50
100
150
Solid: Horizontal
Dots: Vertical
Distance Along 1/3 of Booster Ring in m

Figure 12

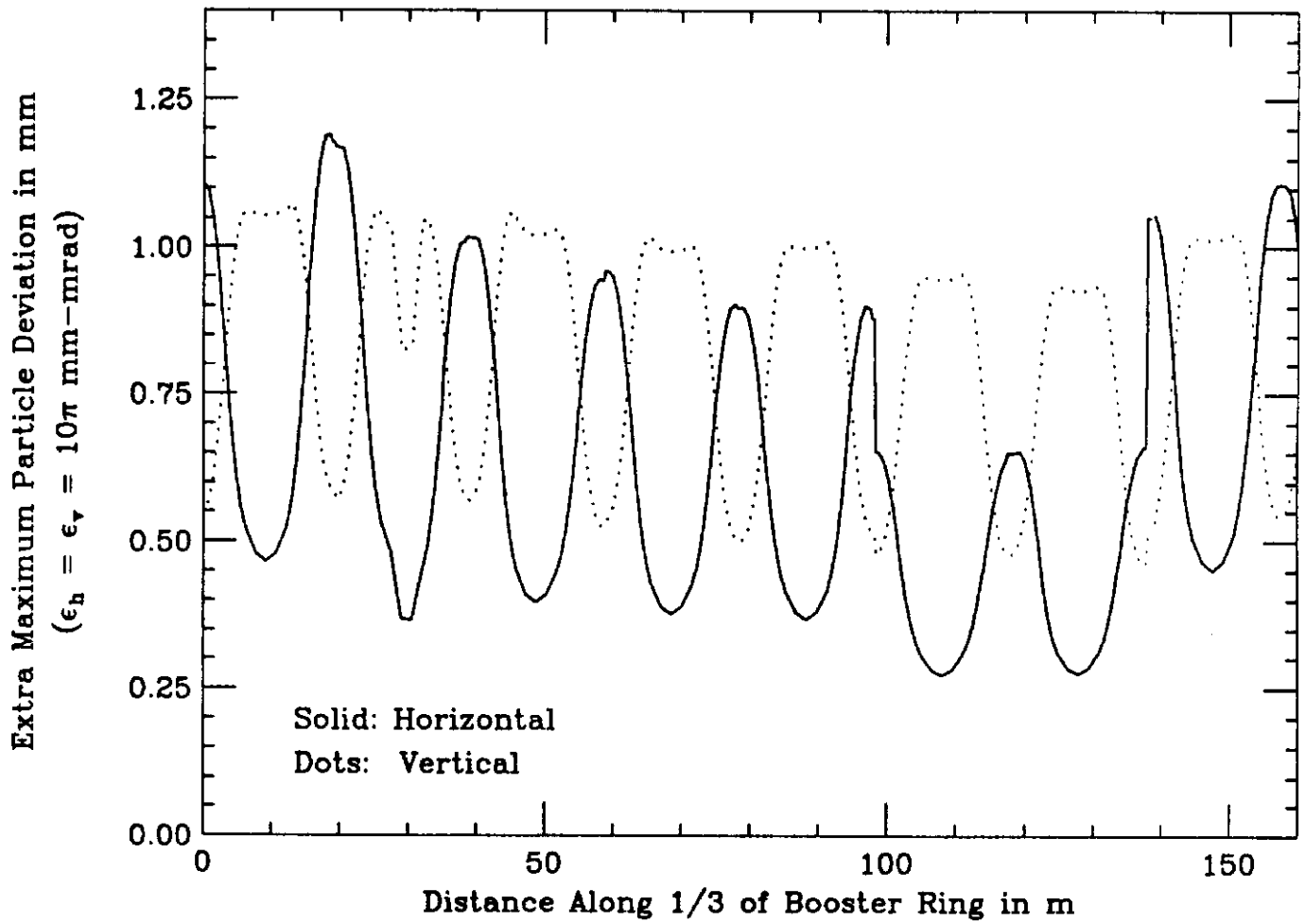
Extra Maximum Particle Deviation in mm
($\epsilon_h = \epsilon_v = 10\pi$ mm-mrad)
1.25
1.00
0.75
0.50
0.25
0.00
0
50
100
150
Solid: Horizontal
Dots: Vertical
Distance Along 1/3 of Booster Ring in m

Figure 13

CONCLUSIONS

Our analysis of the required correcting sextupole strengths, carried out along the momentum ramp with the measured and simulated sextupole excitations of the combined function magnets, concludes that maintaining the net chromaticity at the level set by head-tail instability limits requires much stronger sextupoles. The required sextupole strength is at the level, which can no longer be supported by the present correcting sextupole magnet design. One has to consider either a new iron core sextupole magnet design, or the upgraded air core magnets placed at all accessible high beta locations – the 'enhanced' sextupole layout, which is proposed in this paper. Quantitative assessment of the effect of the stronger compensating sextupoles on the dynamic aperture, carried out in terms of the distortion functions shows that the requisite sextupole configuration would not significantly enhance the third order resonance stop-band – the dynamic aperture remains at acceptable level.

ACKNOWLEDGEMENT

The authors wish to thank Jim Lackey, Chuck Ankenbrandt and Carol Johnstone for discussion and helpful comments.

REFERENCES

1) H. Grote and C. Iselin, *The MAD program users reference guide*, CERN/SL/90-13 (AP), (1990).

2) Y. Chao, FERMILAB, EXP-151, (1987).

3) J. Lackey, Private Communication.

4) E. Willen, P. Dahl and J. Herreza, BNL, AIP Conference Proceedings, (1987).

5) F. Sacherer, Proc. 9-th Int. Conf. on High Energy Accelerators, p. 347, Stanford (1974).

6) S. A. Bogacz, FERMILAB FN-498, (1988).

7) C. Ankenbrandt, Private Communication.

8). T.L. Collins, FERMILAB FN-114, (1984).

9) K-Y. Ng, Proceedings of the 1984 Summer Study on the Design and Utilization of the Superconducting Super Collider, Snowmass, Colorado, (1984).

10) K-Y. Ng FERMILAB TM-1281, (1984)